

Spin temperature concept verified by optical magnetometry of nuclear spins

M. Vladimirova,¹ S. Cronenberger,¹ D. Scalbert,¹ I. I. Ryzhov,²
V. S. Zapasskii,² G. G. Kozlov,¹ A. Lemaître,³ and K. V. Kavokin^{2,4}

¹Laboratoire Charles Coulomb, UMR 5221 CNRS-Université de Montpellier, F-34095, Montpellier, France

²Spin Optics Laboratory, St. Petersburg State University,

1 Ul'yanovskaya, Peterhof, St. Petersburg 198504, Russia

³Centre de Nanosciences et de nanotechnologies - CNRS - Université
Paris-Saclay - Université Paris-Sud, Route de Nozay, 91460 Marcoussis, France

⁴Ioffe Physico-Technical Institute of the RAS, 194021 St.Petersburg, Russia

We develop a method of non-perturbative optical control over adiabatic remagnetisation of the nuclear spin system and apply it to verify the spin temperature concept in GaAs microcavities. The nuclear spin system is shown to exactly follow the predictions of the spin-temperature theory, despite the quadrupole interaction that was earlier reported to disrupt nuclear spin thermalisation. These findings open a way to deep cooling of nuclear spins in semiconductor structures, with a prospect of realisation of nuclear spin-ordered states for high fidelity spin-photon interfaces.

The concept of nuclear spin temperature is one of the cornerstones of the nuclear magnetism in solids^{1,2}. It has made possible realisation of the cryogenic cooling into the microKelvin range³ and observation of nuclear spin ordering in metals and insulators^{4,5}. Such degree of control of the nuclear spin system (NSS) in semiconductor heterostructures would allow enhancing the efficiency of spin-based information storage and processing⁶⁻⁹. However, proving the validity of the spin temperature concept for semiconductor nano- and microstructures is challenging due to the lack of techniques capable of precise sensing of weak nuclear magnetisation in a small volume. In addition, recent experiments showed that in quantum dots, where strong quadrupole-induced local fields have been reported, nuclear spin temperature failed to establish¹⁰. In this context, NSS thermalisation sensing in semiconductor heterostructures is one of the central issues for both fundamental questions related to the realisation of nuclear spin-ordered states, and for potential applications, such as high fidelity spin-photon interfaces⁶⁻⁹.

The basic postulates of the spin temperature theory are illustrated in Fig. 1(a). It is assumed that during the characteristic time T_2 determined by spin-spin interactions the NSS reaches the internal equilibrium. This means that properties of the NSS are governed by a single parameter, the spin temperature Θ_N . When this temperature is made different from the lattice temperature Θ_L (e.g. by the optical pumping), the thermalisation of the NSS with the crystal lattice usually requires a much longer characteristic time T_1 . Fig.1(b) illustrates one of the main predictions of the spin temperature theory: if the NSS is subjected to a slowly varying magnetic field, such that $dB/dt < B_L/T_2$, then Θ_N and the nuclear spin polarisation P_N change obeying universal expressions:

$$\Theta_N / \sqrt{B^2 + B_L^2} = \Theta_{Ni} / B_i; \quad P_N = \frac{B}{3k_B \Theta_N} \hbar \langle \gamma_N (I+1) \rangle. \quad (1)$$

Here γ_N is the gyromagnetic ratio of the nuclear spin I , angular brackets denote the averaging over all nuclear

species, k_B is the Boltzman constant, and Θ_{Ni} is the spin temperature at strong magnetic field $B_i \gg B_L$, where B_L is the local field induced by the fluctuating nuclear spins. These generic relations are based on the principle of entropy conservation in a thermodynamic system during adiabatic process. They constitute the basis for the nuclear spin cooling by adiabatic demagnetisation, a widely used cryogenic technique^{4,11-13}. The nuclear spin temperature may take either positive or negative values, in the latter case the magnetisation being anti-parallel to the applied field.

Various optical and magnetic techniques have been employed to measure nuclear spin temperature, mostly by the magnetisation measurement at a fixed value of the external magnetic field^{4,11,14-16}. On the other hand, a direct measurement of the nuclear magnetisation as a function of slowly varying magnetic field is extremely challenging and has never been realised to the best of our knowledge. Such an experiment is required to check rigorously the validity of the concept of spin temperature as applied to a specific system.

In this Letter we report on realisation of such a proof-of-concept experiment in microcavities, semiconductor microstructures with enhanced light-matter coupling¹⁷. The principle of our experiment is sketched in Fig. 1(c). Prior to the measurement, the NSS of the n-GaAs layer embedded in a microcavity is polarised by optical pumping in the presence of the longitudinal magnetic field. Nuclear spin polarisation is probed by linearly polarized cavity mode photons with the photon energy in the transparency band of GaAs. Polarisation of the light beam transmitted through the cavity is sensitive to the *Overhauser field*, an effective magnetic field created by NSS and acting on electron spins¹⁸. Two methods of detection of nuclear spin polarisation are used: (i) the Faraday effect induced by the Overhauser field^{19,20} and (ii) the spin noise spectroscopy of resident electrons subject to the Overhauser field²¹⁻²³. The main features of the behaviour of the optically cooled NSS under varying external magnetic fields are demonstrated in the experi-

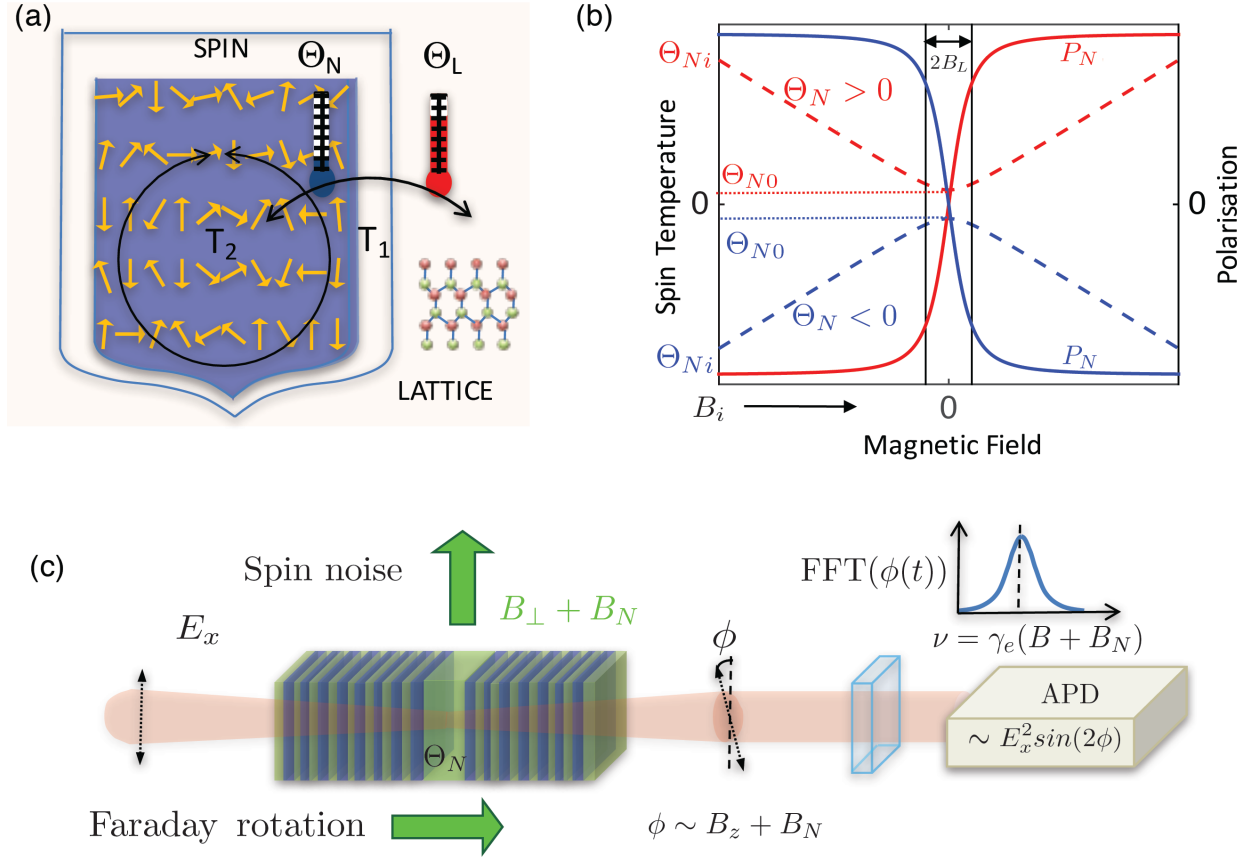


FIG. 1. (a) Sketch of the two heat reservoirs, the atomic lattice at temperature Θ_L , and the nuclear spin system (NSS) at temperature Θ_N . The equilibrium within the NSS is established during the spin-spin relaxation time $T_2 \ll T_1$, the spin-lattice relaxation time. (b) Evolution of the nuclear spin temperature (dashed lines) and polarisation (solid lines) in the adiabatic de(re)-magnetisation process starting from either positive (red lines) or negative initial spin temperature Θ_{Ni} under magnetic field B_i , as described by equation (1). The lowest nuclear spin temperature Θ_{N0} that can be reached in the adiabatic demagnetisation procedure is determined by the initial temperature of the nuclei Θ_{Ni} in the strong magnetic field B_i and the local field B_L . (c) Schematic view of the sample and the detection stage of Faraday rotation and spin noise experiments. NSS in the cavity probed using two optical technics, that allow us to trace the evolution of the initially prepared nuclear spin polarization P_N and temperature Θ_N along the demagnetisation process. Spin noise spectrum is obtained as Fourier transformation of the stochastic Faraday rotation. The spectral peak frequency is directly related to the Overhauser field acting on electrons in the presence of the in-plane magnetic field.

ment where the Faraday rotation angle is measured while ramping the longitudinal magnetic field across zero (Fig. 2). The experiment is conducted in two steps: preparation and measurement (Fig. 2 (a)). The measured signal (Fig. 2(b)) contains two contributions: Faraday rotation directly induced by the external field (shown by solid lines, it remains unchanged for all the scans), and the Faraday rotation induced by the Overhauser field ϕ_N (shown separately in Fig. 2(e) for the first scan), which is proportional to the nuclear spin polarisation. In each consecutive scan, ϕ_N diminishes due to the nuclear spin-lattice relaxation, but the behaviour of nuclear polarisation is described by Eqs. (1): the polarisation is an odd function of the applied field, there is no remanent magnetisation at $B = 0$, and $B_L = 8 \pm 2$ G. We have performed this analysis for two samples with different

concentrations of Si donors n_d : an insulating sample with $n_d = 2 \cdot 10^{15} \text{ cm}^{-3}$ (Sample A) and a sample characterised by a metallic conductivity ($n_d = 2 \cdot 10^{16} \text{ cm}^{-3}$, Sample B), for NSS prepared either at positive, or at negative spin temperature. The value of B_L obtained for both samples is the same within our experimental accuracy.

We complemented these results by spin-noise measurements of nuclear remagnetisation under magnetic field perpendicular to the light and the structure axis (Fig. 3). Color maps in Figs. 3b,c show the evolution of the electron spin noise spectra under varying magnetic fields. The narrow peak in the spectra appears at the frequency ν of the electron Larmor precession in the total effective magnetic field acting upon the electron spins. This field is given by the sum of the external and the Overhauser field, which allows us to extract the nuclear spin polar-

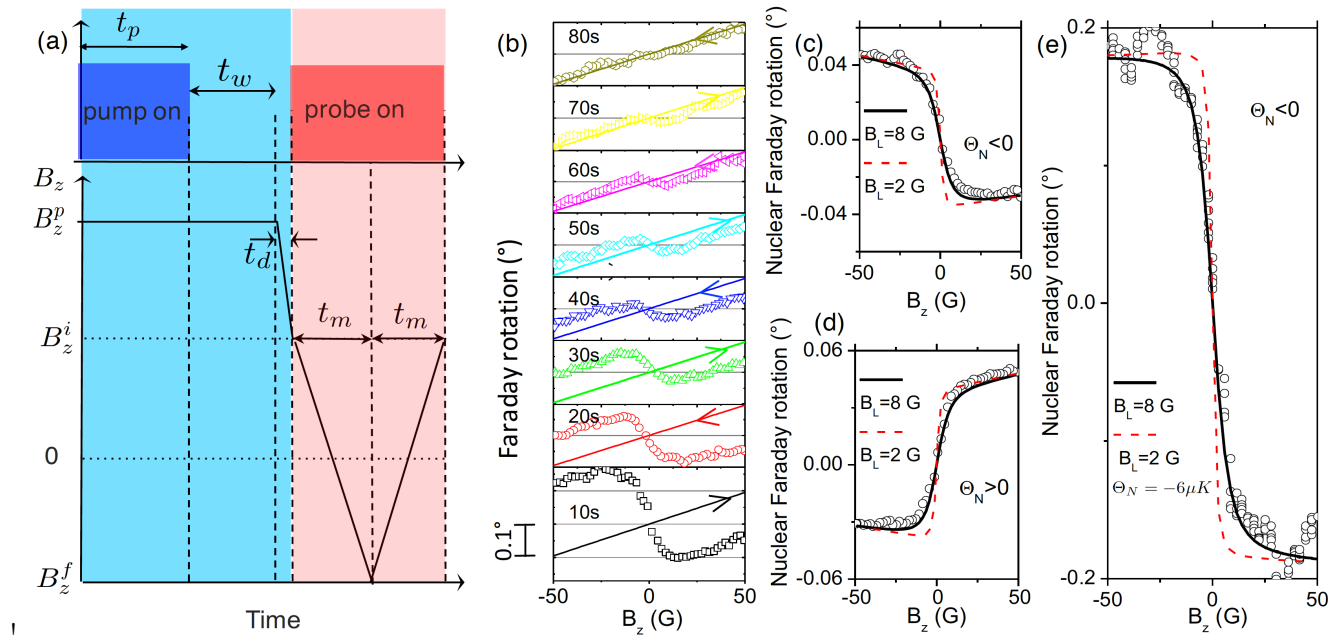


FIG. 2. Nuclear spin magnetometry by Faraday rotation. (a) Timeline of the experiment. The preparation (blue area) consists in pumping under longitudinal magnetic field B_z^p , waiting for eventual nuclear relaxation in the vicinity of the localised electrons during t_w and fast demagnetisation down to B_z^i . Faraday rotation of the probe beam is measured during successive scans of the magnetic field across zero (pink area, only first scan is shown). (b) Raw measurements of the Faraday rotation in Sample B (circles). NSS is prepared at $\Theta_N < 0$. During nine successive scans of the magnetic field ($t_m = 5$ s, direction shown by arrows) conventional Faraday rotation remains constant, this contribution is shown by solid lines. The remaining contribution to the signal is due to the nuclear spin polarisation. It is shown separately in (e) for the first scan. (c-d) Faraday rotation induced in Sample A by nuclear spin prepared either at negative (c) or at positive (d) temperature (circles). Lines in (c-e) are calculated from Eq. (1), assuming different values of the local field, see Supplemental Material (SM).

isation. The asymmetry of the recorded sets of spectra with respect to zero magnetic field is due to nuclear spin-lattice relaxation. We have taken it into account when fitting equation (1) to the data (black dashed lines in Fig. 3(b-e)). For both samples and both signs of the nuclear spin temperature, the value of the local field was found to be $B_L = 12 \pm 2$ G. Thus, the NSS does obey the prediction of the thermodynamic theory expressed by Eq. (1), but value of the local field is surprisingly large, $B_L \approx 10$ G. Indeed, the spin-spin interactions in GaAs are dominated by magnetic dipole-dipole coupling, which yields a much weaker local field $B_{dd} = 1.5 \text{ G}^{24}$.

To elucidate the origin of this striking discrepancy, we performed spin noise measurements with the bulk GaAs layer without a microcavity, Sample C (Fig. 3(f-g)). Although the signal is much weaker, the best fit using Eqs. (1) and taking into account spin-lattice relaxation during the measurement yields $B_L = 2$ G and $\Theta_{N0} = \pm 4 \mu K^{25}$. This comparison shows unambiguously the enhanced value of local field in the microcavities, compared to that in the bulk GaAs. Within the thermodynamic description of the NSS, the local field which enters Eqs. (1) is defined as¹:

$$B_L^2 = \text{Tr}(H_S^2) / \text{Tr}(M_B^2), \quad (2)$$

where H_S is the Hamiltonian of all nuclear spin interactions, excluding Zeeman part (typically it includes the magnetic dipole-dipole interactions, and the indirect exchange), and M_B is the parallel to the magnetic field component of the nuclear magnetic moment. In n-GaAs, magnetic dipole-dipole interaction is well-studied, and $B_L = 2$ G measured in bulk GaAs agrees well with the previous estimations for B_{dd}^{24} .

The only plausible explanation for the unexpectedly strong local field detected in microcavities is the quadrupole splitting $h\nu_Q$ of the nuclear spin states induced by an uniaxial strain. In Eq.(2) it can be accounted for by introducing $H_S = H_{dd} + H_Q$, where H_Q is the Hamiltonian of the quadrupole interaction

$$H_Q = \sum_{i=1}^3 \frac{h\nu_Q^i}{2} (\hat{I}_z^2 - \frac{I(I+1)}{3}). \quad (3)$$

Here the index i stands for the summation over the three isotopes (^{69}Ga , ^{71}Ga , ^{75}As), and \hat{I}_z is the projection on the nuclear spin operator on the growth (strain) axis. Using equation (2) and the parameters of strain-induced quadrupole splittings in GaAs²⁶, one can estimate that the strain as weak as 0.01% induces the local field $B_L = 10$ G in GaAs²⁷.

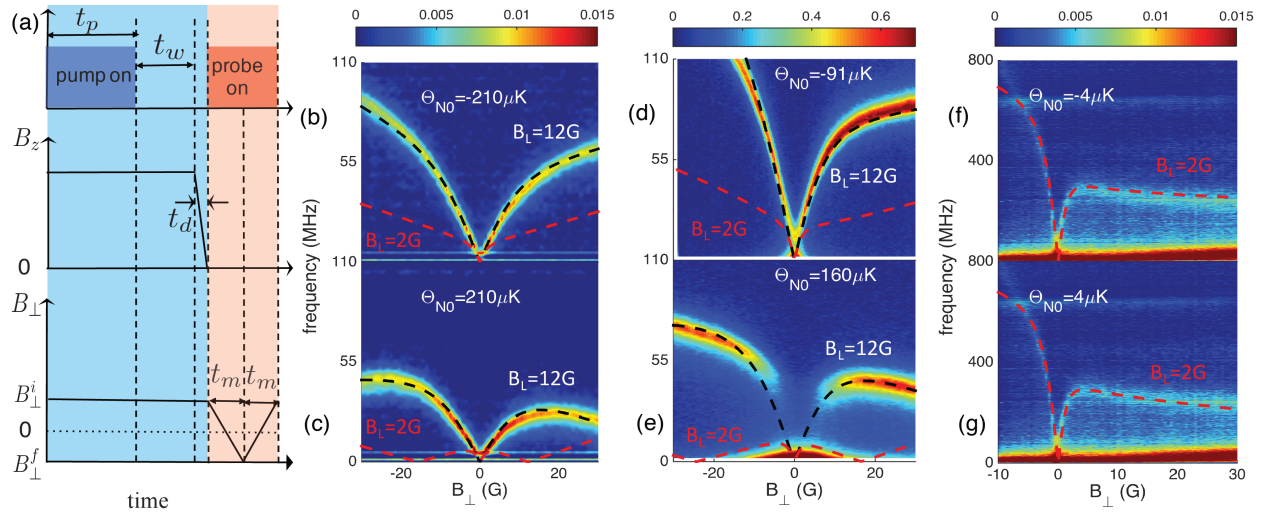


FIG. 3. Nuclear spin magnetometry by spin noise spectroscopy. (a) Timeline of the experiment. The preparation (blue area) consists in pumping under oblique magnetic field, waiting during the time t_w required for nuclear relaxation in the vicinity of localised electrons and fast demagnetisation down to B_\perp^i . Spin noise spectra of the probe beam are measured while scanning B_\perp across zero (pink area). (b-g) Color maps of the spin noise spectra during adiabatic demagnetisation procedure at positive (c, e and g) and negative (b, d and f) spin temperature (measured in the signal to shot noise ratio units) for two microcavity samples A (b-c), B (d-e) and a bulk sample C (f-g). Black lines in (b-e) and red line in (f-g) are fits to Eqs. 1, that determine the values of B_L and Θ_{N0} indicated on the figure (see also SM). Red lines in (b-e) illustrate how the the value $B_L = 2\text{ G}$ fails to describe the experiment.

Because $B_L \gg B_{dd}$, it is the quadrupole interaction that determines the capacity of the NSS to store the energy in the internal degrees of freedom. But in contrast with dipole-dipole interaction, the quadrupole interaction does not provide any coupling between the spins, and can not establish the thermodynamic equilibrium within the NSS. Indeed, in quantum dots, where strong quadrupole-induced local fields have been reported, nuclear spin temperature failed to establish¹⁰. From our data we can estimate the lower limit of 50 G for the *mixing field* B_m , at which Zeeman and internal energy reservoirs come to equilibrium between each other, so that the NSS can be described by the unique spin temperature⁴ (see Supplemental material).

The question remains, how can the thermodynamic equilibrium be established under magnetic field $B_m > 50\text{ G}$, much larger than the characteristic field of the dipole-dipole interaction $B_{dd} = 1.5\text{ G}$? We suggest that this is made possible by the multi-isotope nature of the NSS in GaAs. The difference in the quadrupole splittings and gyromagnetic ratios between the three isotopes yields a rich variety of possible inter-isotope flip-flop transitions. These transitions frequencies ν_N are illustrated in Fig. 4 as functions of the magnetic field in the absence (Fig. 4a) and in the presence of the quadrupole splitting of the nuclear spin states along z -axis (Fig. 4 (c, e)). The spin flip-flop transitions involving different isotopes ensure the energy transfer between the Zeeman and quadrupole energy reservoirs, with total energy conservation of the NSS.

These transitions are broadened by dipole-dipole interactions. It is usually assumed⁴ that the efficient equilibration of energy reservoirs is ensured at detuning from the resonance less than $\delta\nu_N = 5B_{dd}/(2\pi\langle\gamma_N\rangle) = 8\text{ kHz}$. One can see in Fig. 3d,f, that for both orientations of the magnetic field, the transitions involving such a small detuning are available at $B < 50\text{ G}$, and the mixing remains as efficient as in the absence of the quadrupole splitting (Fig. 3(b)).

Our results show that the strain-induced nuclear quadrupole splittings in semiconductor microcavity do not hinder the establishment of the thermodynamic equilibrium within the nuclear spin system. The quadrupole effects result in the increase of the local field, indicating that the heat capacity of the NSS is dominated by the quadrupole energy reservoir. The energy transfer between the Zeeman and quadrupole reservoirs during adiabatic demagnetisation is made possible by dipole-dipole interaction via spin flip-flop transitions involving different isotopes. Thus, deep cooling of the NSS down to microKelvin temperature range via adiabatic demagnetisation is possible in photonic microstructures. This paves the way towards realisation of nuclear magnetically ordered states and their applications, including spin-photon interfaces with reduced thermal noise.

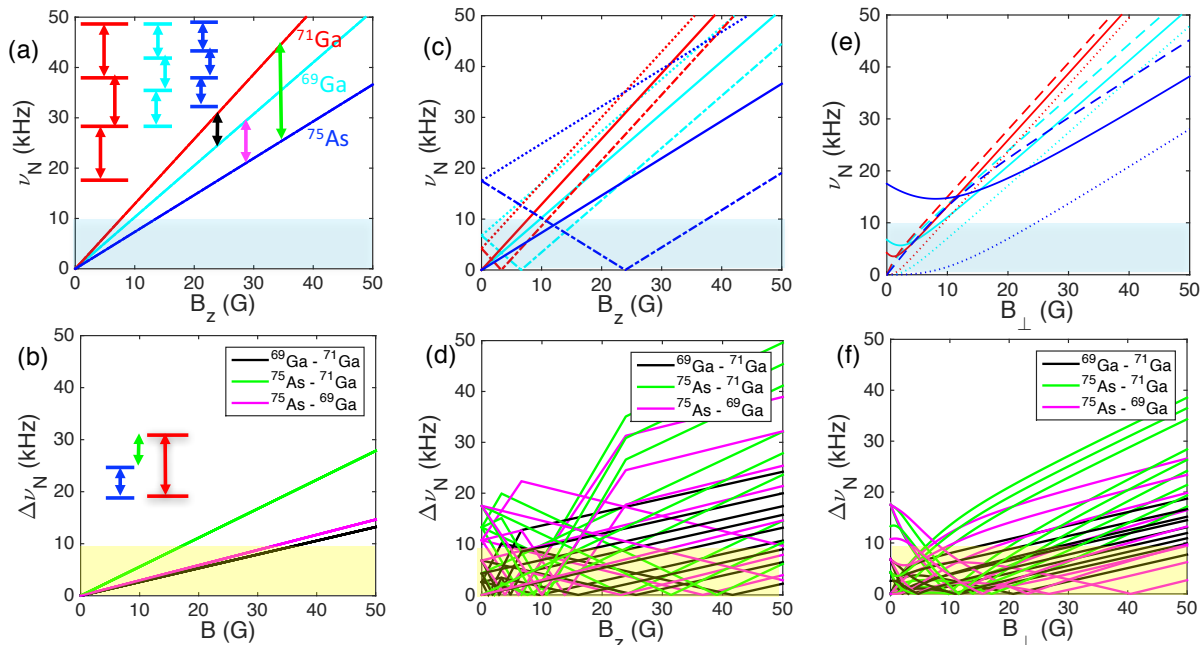


FIG. 4. (a) Nuclear spin flip transition frequencies ν_N for three GaAs isotopes, and (b) the differences $\Delta\nu_N$ between them as functions of magnetic field in the absence of the quadrupole splitting. (c, d) Same as (a) and (b), respectively, but in the presence of the quadrupole splitting in z -direction. (d, f), Same as (c) and (d), respectively, but the magnetic field is applied in the plane of the structure. The blue area $\nu_N < 8$ KHz in (a, c, d) shows the extent of splittings in the local magneto-dipole field and indicates the range of external fields where mixing is possible within each individual isotope. Similarly, the yellow area in (b, d, f) indicates the range of magnetic fields where mixing becomes possible if assisted by inter-isotope transitions.

ACKNOWLEDGMENTS

This work was supported by the joint grant of the Russian Foundation for Basic Research (RFBR, Grant No. 16-52-150008) and National Center for Scientific Research (CNRS, PRC SPINCOOL No. 148362), as well as

French National Research Agency (Grant OBELIX, No. ANR-15-CE30-0020-02). IIR, VSZ and GGK acknowledge Russian Foundation for Basic Research (grant No. 17-12-01124) for the financial support of their experimental work.

Supplemental Material

I. SAMPLES

The studied microcavity structures consist of Si-doped GaAs $3\lambda/2$ -cavity with electron concentrations $n_e = 2 \times 10^{15} \text{ cm}^{-3}$ (Sample A) and $n_e = 4 \times 10^{16} \text{ cm}^{-3}$ (Sample B). The front (back) mirrors are distributed Bragg reflectors composed of 25 (30) pairs of AlAs/Al_{0.1}Ga_{0.9}As layers, grown on a 400 μm thick GaAs substrate. Due to multiple round trips in the cavity, the Faraday rotation (FR) is amplified by a factor of $N \sim 1000$, corresponding to the interaction length $L = 0.7 \text{ mm}$ (quality factor $Q \sim 20000$ was measured by interferometric techniques) Sample C is the bulk 20 μm -thick GaAs layer grown by liquid-phase epitaxy, with Si donor concentration of $n_d = 4 \times 10^{15} \text{ cm}^{-3}$. All these samples have been studied previously^{20,21,28,29}.

II. EXPERIMENTAL TECHNIQUES

Both the spin-noise (SN) and FR techniques have been used previously for studies of the NSS^{20,21,29} and are described in detail in Ref. 29. They have an advantage of being virtually non-perturbative for the NSS, because pumping and measurement stages are separated in time, and cooled NSS is optically probed via the polarisation

rotation of the light beam with photon energy tuned below (here 20 meV) the band gap of the studied GaAs layer. In a typical measurement, the sample is placed in a cold finger cryostat at $T = 5$ K, $B_z = 180$ G. At the first stage, it is optically pumped during 3-15 minutes by the circularly polarised laser diode with photon energy 1.57 eV and power $P = 10$ mW, focused on 1 mm spot on the sample surface. In the case of SN experiments, the transverse field B_\perp is also applied during pumping. After the pumping stage, we wait for $t_w = 1$ minute before lowering down B_z (Fig. 2(a), 3(a)), to be sure that nuclear spins situated under the orbits of the donors and characterised by the relatively short T_1 do not contribute to the signal^{20,21,23}. At the last preparation step, B_z is lowering down to the value from which the measurement stage starts ($B_z = B_z^i = 50$ G for FR and $B_z = 0$ for SN). FR and SN experiments mainly differ by the measurement stage. In FR experiment, the rotation of the linearly polarised probe beam is detected in the presence of the slowly varying longitudinal magnetic field B_z . In the SN experiment, the spin noise of the resident electrons is measured in the presence of the slowly varying transverse magnetic field B_\perp via the fluctuation spectrum of the Faraday rotation angle. The probe beam has the photon energy 20 meV below GaAs band gap, power of 0.5 mW, and is focused on 30 μm spot on the sample surface.

II.1. Faraday rotation

To extract nuclear spin temperature and the local field from the Faraday rotation angle measured as a function of the slowly varying magnetic field B_z (the duration of each scan is ~ 10 s so that $dB/dt = 10$ G/s), we proceed as follows. First, we subtract the external field contribution from the total signal. This contribution to the signal remains unchanged for all consecutive scans and depends linearly on the magnetic field. The remaining part of the FR is induced by the Overhauser field B_N , which is proportional to the nuclear spin polarisation P_N .

$$\phi_N = B_N V_N L = b_N P_N V_N L, \quad (\text{S1})$$

where $b_N = 5.3$ T is the Overhauser field produced by the fully polarised nuclear spins¹⁸, V_N is the nuclear Verdet constant, L is the effective optical length of the sample accounting for by multiple round trips of light in the cavity²⁰. Therefore, from Eqs. (1) we get:

$$\phi_N = \phi_{Ni} B / \sqrt{B^2 + B_L^2} \quad (\text{S2})$$

where ϕ_{Ni} is the Faraday rotation angle at the saturation field B_z^i . Fitting ϕ_N to equation (S2) we determine $B_L = 8 \pm 2$ G. Using the values of $V_N = 0.1$ mrad/G/cm and $L = 0.7$ mm determined in our previous work²⁰ we also extract $\Theta_{N0} = -6$ μK in sample B (Fig. 2 (e) in the main text) from Eqs. (S1), (S2) and (1). The values of B_L and Θ_{N0} extracted from FR measurement are averaged over the crystal volume, since the signal is given by the electron band spin splitting²⁰.

II.2. Spin noise spectroscopy

The electron spin noise spectrum exhibits a pronounced peak at the electron Larmor frequency ν corresponding to the total (B_\perp and B_N) field, so that:^{21,23}

$$\nu = \gamma_e (B_\perp + B_N) = \gamma_e (B_\perp + b_N P_N), \quad (\text{S3})$$

where $\gamma_e = 0.64$ MHz/G is the gyromagnetic ratio of the electrons in the conduction band of GaAs²¹. Thus, by measuring ν as a function of B_\perp and fitting equations (1) and (S3) to the data we obtain the values of Θ_{N0} and B_L . Because each field scan takes 100 s (10 times longer than in the case of the Faraday rotation measurements), the spin-lattice relaxation of the NSS is not negligible on this time-scale. It manifests itself in the asymmetry of the recorded sets of spectra with respect to zero magnetic field. For the quantitative comparison with the theory predictions given by Eqs. (1) and (S3) we measured the magnetic field-dependent relaxation times in an independent set of experiments²⁹. Note that in metallic samples the SN signal is mediated by the electron gas, and is therefore contributed by all the nuclei. In the insulating samples, only the nuclei situated under the donor orbits can be detected. However, the polarisation of the nuclear spins situated in the core of the donor orbit decays rapidly, and vanishes during t_w . Thus the SN signal comes from the nuclei situated in the periphery of the donor orbits, so that the extracted Θ_{N0} and B_L are close to those of the bulk nuclei.

III. ESTIMATION OF THE MIXING FIELD

The mixing field B_m , is the field at which Zeeman (for each of three isotopes) and internal energy reservoirs come to equilibrium between each other⁴. Only the Zeeman reservoirs can be cooled down via dynamic nuclear polarisation at strong field. By measuring nuclear polarisation, we get access to the average energy of the Zeeman reservoirs $\langle E_Z \rangle = BP_N \langle \hbar \gamma_N \rangle$. During adiabatic demagnetisation, energy transfer and the thermalisation between Zeeman and internal energy reservoirs is achieved at $B = B_m$. At this field, a part of Zeeman energy is transferred to the internal energy reservoir, which results in the modification of the nuclear polarisation. The nonadiabaticity of this process would lead to a deviation from Eqs. (1), quantified by the nonadiabaticity factor $f_{na} = B_m / \sqrt{B^2 + B_m^2}$ ⁴. Comparing the magnetisation measured at $B = 50$ G before and after the passage through zero field, we have not observed any difference within the experimental precision of 2%. This yields $f_{na} > 0.98$, and therefore $B_m > 50$ G.

-
- ¹ M. Goldman, *Spin temperature and nuclear magnetic resonance in solids*, International series of monographs on physics (Clarendon Press, 1970).
- ² A. Abragam and W. G. Proctor, *Physical Review* **109**, 1441 (1958).
- ³ G. R. Pickett, *Rep. Prog. Phys.* **51**, 1295 (1988).
- ⁴ A. S. Oja and O. V. Lounasmaa, *Rev. Mod. Phys.* **69**, 1 (1997).
- ⁵ A. Abragam, *The Principles of Nuclear Magnetism* (Oxford University Press, Oxford, 1961).
- ⁶ C. Arnold, J. Demory, V. Loo, A. Lemaître, I. Sagnes, M. Glazov, O. Krebs, P. Voisin, P. Senellart, and L. Lanco, *Nature Communications* **6**, 6236 (2015).
- ⁷ R. Stockill, C. Le Gall, C. Matthiesen, L. Huthmacher, E. Clarke, M. Hugues, and M. Atatüre, *Nature Communications* **7**, 12745 (2016).
- ⁸ S. Sun, H. Kim, G. S. Solomon, and E. Waks, *Nature Nanotech* **11**, 539 (2016).
- ⁹ W. B. Gao, P. Fallahi, E. Togan, J. Miguel-Sanchez, and A. Imamoglu, *Nature* **491**, 426 (2012).
- ¹⁰ P. Maletinsky, M. Kroner, and A. Imamoglu, *Nat Phys* **5**, 407 (2009).
- ¹¹ J. Tuoriniemi, *Nat Phys* **12**, 11 (2016).
- ¹² F. Pobell, *Matter and Methods at Low Temperatures*, 3rd ed. (Springer-Verlag, 2007).
- ¹³ N. Kurti, F. N. H. Robinson, F. Simon, and D. A. Spohr, *Nature* **178**, 450 (1956).
- ¹⁴ M. Chapellier, M. Goldman, V. H. Chau, and A. Abragam, *J. Appl. Phys.* **41**, 849 (1970).
- ¹⁵ M. Goldman, M. Chapellier, V. H. Chau, and A. Abragam, *Phys. Rev. B* **10**, 226 (1974).
- ¹⁶ E. A. Chekhovich, A. Ulhaq, E. Zallo, F. Ding, O. G. Schmidt, and M. S. Skolnick, *ArXiv e-prints* (2017), arXiv:1701.02759 [cond-mat.mes-hall].
- ¹⁷ A. Kavokin, J. J. Baumberg, G. Malpuech, and F. P. Laussy, *Microcavities*, Series on Semiconductor Science and Technology (OUP Oxford, 2007).
- ¹⁸ F. Meier and B. Zakharchenya, eds., *Optical orientation*, Modern Problems in Condensed Matter Science Series, Vol. 8 (North-Holland, Amsterdam, 1984).
- ¹⁹ E. Artemova and I. Merkulov, *Sov. Phys. Solid State* **27**, 941 (1985).
- ²⁰ R. Giri, S. Cronenberger, M. M. Glazov, K. V. Kavokin, A. Lemaître, J. Bloch, M. Vladimirova, and D. Scalbert, *Phys. Rev. Lett.* **111**, 087603 (2013).
- ²¹ I. I. Ryzhov, S. V. Poltavtsev, K. V. Kavokin, M. M. Glazov, G. G. Kozlov, M. Vladimirova, D. Scalbert, S. Cronenberger, A. V. Kavokin, A. Lemaître, J. Bloch, and V. S. Zapasskii, *Appl. Phys. Lett.* **106**, 242405 (2015).
- ²² F. Berski, J. Hübner, M. Oestreich, A. Ludwig, A. D. Wieck, and M. Glazov, *Phys. Rev. Lett.* **115**, 176601 (2015).
- ²³ I. I. Ryzhov, G. G. Kozlov, D. S. Smirnov, M. M. Glazov, Y. P. Efimov, S. A. Eliseev, V. A. Lovtcius, V. V. Petrov, K. V. Kavokin, A. V. Kavokin, and V. S. Zapasskii, *Sci. Rep.* **6**, 21062 (2016).
- ²⁴ D. Paget, G. Lampel, B. Sapoval, and V. Safarov, *Physical Review B* **15**, 5780 (1977).
- ²⁵ See details in Supplemental Material.
- ²⁶ K. Flisinski, I. Y. Gerlovin, I. V. Ignatiev, M. Y. Petrov, S. Y. Verbin, D. R. Yakovlev, D. Reuter, A. D. Wieck, and M. Bayer, *Phys. Rev. B* **82**, 081308 (2010).
- ²⁷ M. Eickhoff, B. Lenzmann, D. Suter, S. E. Hayes, and A. D. Wieck, *Phys. Rev. B* **67**, 085308 (2003).
- ²⁸ M. Kotur, R. I. Dzhiyev, M. Vladimirova, B. Jouault, V. L. Korenev, and K. V. Kavokin, *Phys. Rev. B* **94**, 081201 (2016).
- ²⁹ M. Vladimirova, S. Cronenberger, D. Scalbert, M. Kotur, R. I. Dzhiyev, I. I. Ryzhov, G. G. Kozlov, V. S. Zapasskii, A. Lemaître, and K. V. Kavokin, *Phys. Rev. B* **95**, 125312 (2017).